

DOI: 10.1002/ ((please add manuscript number))

Article type: Full Paper

Fracture properties of Graphene-coated Silicon for photovoltaics

Brahmanandam Javvaji, Pattabhi Ramaiah Budarapu, Marco Paggi*, Xiaoying Zhuang and Timon Rabczuk*

Dr. B. Javvaji, Prof. X. Zhuang
Institute of Continuum Mechanics, Leibniz Universität Hannover, Appelstr. 11, D-30167
Hannover, Germany

Dr. P. R. Budarapu
School of Mechanical Sciences, Indian Institute of Technology, Bhuaneswar 751007, India
E-mail: pattabhi@iitbbs.ac.in

Dr. P. R. Budarapu, Prof. M. Paggi
IMT School for Advanced Studies Lucca, Piazza San Francesco 19, 55100 Lucca, Italy
E-mail: marco.paggi@imtlucca.it

Prof. T. Rabczuk
Institute of Structural Mechanics, Bauhaus University of Weimar, 99423 Weimar, Germany

Keywords: graphene, silicon, graphene deposited silicon, molecular dynamics, photovoltaic solar cells

The possibility to replace the conductive gridline deposited on solar cells by highly electrically conductive Graphene is opening new perspectives for the future generation of photovoltaics. Beside the enhanced electric performance, Graphene can also have a role on the resistance of Silicon against cracking. Here, the influence of depositing Graphene on the Silicon surface, on the fracture properties of Silicon has been investigated. To pin-point the influence of Graphene, fracture properties estimated from molecular dynamics simulations of three different cases in uni-axial tension are compared. In the first case, the fracture properties of Silicon alone are estimated in relation to different initial defect sizes. Secondly, the same simulations are repeated by depositing Graphene on the Silicon surface. Atomic interactions in the composite structure are modeled using the combined AIREBO and Tersoff potential functions. Improvement of about 780% in the Young's modulus of Silicon is achieved after coating with Graphene. Furthermore, to study the influence of realistic initial defects in

Graphene, a third set of simulations is considered by repeating the previous tests but with initial cracks through Graphene and Silicon. Predictions show that Graphene can be highly beneficial in strengthening and repairing micro-cracked Silicon to decrease electrical power losses caused by cracks.

1. Introduction

The renewable, non-polluting and clean nature of the solar energy makes it one of the fast growing technology in the World.^[1] Photovoltaic (PV) solar cells made of Silicon (Si) (see **Figure 1a**), play a key role in converting solar energy into electricity based on the PV effect of Silicon semiconductor. Standard PV modules are laminates composed of: (i) a glass superstrate, (ii) an encapsulating polymer layer like ethylene vinyl acetate (EVA), (iii) a layer of Si solar cells, (iv) a second layer of EVA, and finally (v) a thin multi-layered backsheets,^[2] see **Figure 1a**. Two main semiconductors, called bus-bars, connect the cells together, while a finer gridline of tiny conductors, called fingers, have the role to collect the generated currents from Silicon and transport them to the bus-bars.

The present theoretical and applied research has mostly focused on increasing the solar energy conversion efficiency of the cells.^[3,4] Although efficiencies up to 40% have been reached in the laboratory using single junction Gallium Arsenide (GaAs) and multi-junction concentrators,^[5] the technology based on mono- and poly-crystalline Si is still the most competitive on the market, due to the low price of Si semiconductor and the widely established material processing developed in the field of electronics.^[6] Therefore, researchers have attempted to develop new technologies^[7] based on thinner and thinner Silicon layers^[8-11] and thin films to save material, although these solutions will be even more prone to cracking than standard solar cells. New kinds of cell structures and coatings are also explored^[12,13] to achieve higher solar energy conversion efficiencies. In this context, research on the durability of PV modules is an area not much investigated yet, though it is relevant for the feasibility

analysis of new solar cell architectures. The study of durability of PV modules requires the characterization of the effect of micro-cracking induced by mechanical loads and thermal variations on the electric response of the solar panel. Therefore, in order to efficiently tackle this issue, interdisciplinary research including disciplines from structural mechanics to solid state physics is required.

Due to small thickness and brittle nature of Silicon, cracks are prone to develop during production, transportation, installation and operation. Cracking hinders the progress towards the use of thinner Silicon wafers. The durability of PV devices is mainly affected by cracking in Silicon due to thermo-mechanical loading.^[14] Cracks can interrupt the grid line deposited on solar cells, creating large portions of electrically insulated areas.^[15,16] **Figure 1b** shows the electrical response and crack pattern during a bending test of solar cells.^[17] Dark areas highlighted in the dotted circle of the loaded configuration in **Figure 1b** indicate the electrically inactive regions, which are not seen in the unloaded configuration. In spite of the new and efficient manufacturing techniques to reduce the number of cells/modules rejected by quality control,^[18,19] it is impossible to avoid the occurrence of micro-cracking due to the brittleness of Silicon. Qualification standards IEC 61215 require passing of severe laboratory tests in an artificial climate chamber. However, micro-cracking is not yet used as a quantitative indicator for the quality assessment of PV modules.

Kajari et al.^[20] have analyzed micro-cracking resulting from snow tests and artificial aging in the laboratory using the electroluminescence (EL) technique. Micro-cracking can lead to large electrically disconnected cell areas (see e.g. **Figure 1b**), with up to 21% of power-loss.^[15,21–24] Furthermore, orientation of cracks with respect to the bus-bars plays a key role in determining their criticality.^[21] A micro-cracked cell shows also a local increase of operating temperature near the crack, as highlighted from molecular dynamics^[25] and also finite element method^[26] based simulations. Thermographic studies show that cracks are acting primarily as recombination centers with a local increase in temperature around them.^[26]

Deformations are also induced by the night and day variation in temperature. Moreover, temperature affects the electric performance of the PV module, since the electrical output of the semiconductor exponentially varies with temperature.^[27,28]

Paggi et al.^[17] demonstrated the complex interaction between crack propagation in mono-crystalline Silicon cells embedded in PV modules and the electric output, based on an experimental study using EL technique. They proved that, due to the action of the encapsulating polymer and residual thermo-elastic stresses, cracked regions can partially recover the electric conductivity during mechanical unloading due to crack closure, apart from reporting fatigue degradation during cyclic bending. Berardone et al.^[23] have developed a one-dimensional model for simulating the electric current distribution in solar cells accounting for a distributed series resistance in the presence of partially conductive cracks. This can be included in a multi-physics and multi-scale computational approach to study the evolution of microcracking in polycrystalline Silicon (Si) solar cells in PV modules, as proposed in.^[28]

The generated electricity in a solar cell is transmitted through the fingers, which are further connected to the external load through the bus-bars. Fingers are firmly attached to the Silicon surface on top of the p-n junction. When the micro-cracks in solar cell are parallel to the bus-bars, area not available for power production (highlighted as dark patch in **Figure 1b**) is significant. The mono-layer Graphene is an extremely conductive, highly transparent material with extreme mechanical properties.^[25] Therefore, when Graphene is bonded to the surface of the Silicon, the composite cell is expected to have better mechanical and electrical properties compared to Silicon alone. Due to the Carbon-to-Silicon atomic interactions on the surface of Graphene deposited Silicon, the Carbon atom orbital symmetry will be broken, which introduces the electronic bandgap.^[29,30] Therefore, the interaction field near the Graphene-Silicon interface efficiently separates the electron-hole pair created by the absorption of quantum mechanical energy and thus induce the photocurrent.^[31,32] As a

consequences of the interface interactions between Graphene and Silicon, several other applications, such as: photodetectors,^[33,34] electrodes,^[35] field-effect-transistors,^[36] heterojunction diodes,^[37] to name a few, can be realised. Moreover, the compressive residual thermo-elastic stresses in the cell are expected to increase, inducing crack closure effects. The advantages include: (i) large portions of electrically inactive solar cells can be avoided. (ii) Due to the super conducting nature of Graphene, it is particularly easy to trap the generated power. (iii) Since, there are no joints involved when Graphene is coated on Silicon, no soldering is required, which will significantly reduce the stress concentration points and hence the probability of generation of new cracks.

In this study, we investigate the effect of depositing Graphene on Silicon surface to enhance its fracture properties. To this aim, molecular dynamics simulations are carried out to perform virtual uni-axial tensile tests. All the simulations are performed using the open source Large-scale Atomic/Molecular Massively Parallel Simulator (LAMMPS).^[38] To the best knowledge of the authors, the proposed methodology is the first of its kind. The article is structured as follows: details of modeling the composite structure and simulation steps are discussed in “Modelling and simulation” section. The influence of depositing Graphene on Silicon surface is studied based on the uni-axial tensile tests of three different cases. The corresponding results are discussed in “Results and discussion” section and the key contributions are summarised in “Conclusions” section.

2. Modeling and simulation

Considering the extraordinary mechanical and electrical properties of Graphene, we propose to deposit Graphene on Silicon surface, which aids in arresting the crack growth in Silicon, particularly used in the photovoltaic solar cells. The enhancement in the fracture properties of Silicon is estimated based on the molecular dynamics (MD) simulations. In the MD simulations, perfect coupling is ensured by bonding the Carbon atoms in Graphene with the surface atoms of Silicon. Furthermore, in order to pin-point the influence of Graphene, three

different MD models are considered: (i) Silicon alone, (ii) Silicon deposited with defect free Graphene and (iii) Silicon deposited with Graphene containing initial notch. Therefore, three different types of atomic interactions are possible: (i) Silicon to Silicon, (ii) Carbon to Carbon and (iii) Carbon to Silicon.

The atom-to-atom interactions are simulated through a combination of Adaptive Inter-molecular Reactive Empirical Bond Order (AIREBO)^[39] and Tersoff^[40] potential functions. The stability and deformation characteristics of Silicon and Silicon carbide systems can be accurately predicted by Tersoff potential function.^[40] On the other hand, AIREBO potential function has been successfully employed to capture the mechanical properties of hydrocarbons,^[39] graphite^[41] and carbon nanotubes.^[42] Furthermore, in the present Silicon-Graphene system there exist bonded and non-bonded types of interactions between Silicon and Carbon atoms. The bonded interactions are simulated using the Tersoff potential function, whereas, the non-bonded interactions are modeled using the short-range Lennard-Jones potential function.^[43] Such a combination potential has been successfully employed in capturing the dynamics of Silicon and Carbon composite system, to simulate the thermal transport between Graphene and Silicon carbide surface,^[44] bombardment of Silicon ions with Graphene^[45] and to estimate the stable configuration of Graphene on Silicon surface.^[46] Recent progress in the treatment of non-bonded interactions using first principle theory^[47] and variational approach^[48] can further elucidate the insights to this. The detailed information about AIREBO and Tersoff potential functions and the numerical values for parameters can be found in.^[39,40] The cut-off function in the AIREBO potential is modified to 1.95 Å to avoid the high tensile forces of broken carbon bonds.^[49-52]

In order to estimate the fracture properties of composite Graphene-Silicon system, three different cases are considered as shown in **Figure 2**. In the first case shown in **Figure 2a**, the fracture properties of Silicon alone are estimated with various initial notch sizes. Secondly, the simulations in the first case are repeated by bonding the defect free Graphene

on the Silicon surface, refer to **Figure 2b**. Finally, to investigate the influence of Graphene with defects, the simulations in the second case are repeated considering an initial notch in Graphene as well, see **Figure 2c**. In **Figure 2**, the solid-dash line indicates the initial crack surface and the carbon atoms on the crack surface are highlighted. A $156 \text{ \AA} \times 156 \text{ \AA}$ single layer Graphene sheet is bonded to a Silicon (001) substrate of dimensions $156 \text{ \AA} \times 156 \text{ \AA} \times 16 \text{ \AA}$, where the centers of both Graphene and Silicon are aligned in the middle of the domain. The Graphene is initially separated at a distance of 1.663 \AA from Silicon surface. This is found to be the optimum distance of separation, where the interactions between Silicon and Carbon are reported to be converging.^[46] As shown in **Figure 2**, the top and bottom rows of atoms are prescribed with a tensile load (P), whereas, the left and right edge atoms are allowed to move only along the vertical direction. The tensile load is specified in cycles, where each cycle consists of loading for a period of 1 ps followed by a relaxation of 1 ps. The total stress, fracture stress, fracture strain and the potential energy at fracture are estimated based on the deformed configuration.

3. Results and discussion

In this section, results of the three different cases (see **Figure 2**) considered in this study are summarised and discussed. Distribution of the Young's modulus for various cases is listed in **Table 1**. According to **Table 1**, considering un-notched specimens, the improvement in Young's modulus with and without Graphene is estimated to be 754%. On the other hand, considering a 20% initial notch in Silicon alone and Silicon and Graphene composite (between case 1 and case 2), the improvement in Young's modulus is observed to be 786%. Finally, considering the 20% initial notch in Silicon and Graphene composite (among case 1 and case 3), the improvement in Young's modulus as compared to 20% crack in Silicon alone is estimated to be 694%. Therefore, the enhancement in the mechanical properties of the Graphene deposited Silicon composite for case 2 system is the highest. This is due to the significantly high fracture strength of pristine Graphene, compared to Silicon. In case 2, the

crack growth in the composite will not initiate until the first cracks are initiated in the pristine Graphene. However, the enhancement in fracture strength is significant in general for all case 2 and case 3.

The crack growth simulations with Silicon alone (see **Figure 2a** for case 1 schematic), were performed considering 7 different initial notch sizes. Distribution of the system potential energy and the stress along the y direction vs. the strain along the y direction are plotted in **Figure 3a-b**, respectively. According to **Figure 3**, the fracture strength and the peak potential energy are observed to be decreasing with increase in initial notch size. The yield stress and yield strain are the stress and strain values captured at the time of first bond break. This is indicated by a drop in the potential energy and the stress. The deformed configurations at selected strains for an initial notch size of 0.2L as mentioned in the inset of **Figure 3b** are shown in **Figure 4a-c**. They also correspond to specific strains of 0.165, 0.192, 0.197, indicated by points A, B and C, respectively, on the stress-strain curve highlighted in the closeup of **Figure 3b**. Based on **Figure 4a-c**, the bond breaking and hence the crack growth are evident in Silicon alone (case 1) as the time progresses. Furthermore, per atom stresses indicated by different atom colours and the colour bar, are superposed in the deformed configurations in **Figure 4**. The deformed configuration in **Figure 4a** corresponds to point A in the inset of **Figure 3b**, which represent the breakage of first bonds between the Silicon atoms. Therefore, the corresponding local atomic rearrangement results in the drop of the stress from 5.849 to 5.832 GPa, see the closeup in **Figure 3b**. In this study, the first drop in the stress corresponding to point A is considered as the yield point. Further application of the load leads to a semi-stable atomic configuration, where the stress is observed to increasing from point A to point B. Between these points, no further yielding was observed, whereas, the load is transferred to the neighbouring atoms. The atomic configuration in **Figure 4a-b** supports this observation. Therefore, bond elongation and reorientation are noticed as the load increases from point A to point B. The bond length reaches a threshold value at point B,

followed by the bond breakage indicated by sudden drop in the potential energy and the stress, see **Figure 3**. Further loading resulted in the rapid bond breakage induced crack growth, evidenced through the breakage of several bonds along the x direction as shown in **Figure 4c**, leading to the fracture of Silicon. Similar crack growth mechanics are observed for other initial notch sizes as well. However, the slopes in stress-strain curves shown in **Figure 3b** are observed to decrease, particularly at large strains, with the increase in size of the initial notch.

The simulation results of stress, strain and potential energy of un-notched Graphene deposited on Silicon surface (case 2) are plotted in **Figure 5**, which are compared to the results of crack growth in pure Silicon. An observation of the potential energy and stress distribution indicate the first drop in un-notched Graphene deposited on Silicon is greater than the Silicon alone. Therefore, depositing Graphene on the Silicon surface strengthens Silicon, resulting in large deformations before failure. The deformed configurations of un-notched Graphene deposited on Silicon surface considering an initial notch size of $a = 0.2L$, at specific points of time 40.0 ps, 41.3 ps, 45.8 ps and strains 0.255, 0.263 and 0.293, are plotted in **Figure 4d-f**, respectively. **Figure 4d** is captured at the time of first bond breakage. The strain at the time of first bond breakage is 1.5 times larger for Graphene deposited Silicon, as compared to the Silicon alone. Therefore, it is evident that the first bond breakage observed in **Figure 4a** is prolonged by depositing the Graphene on Silicon surface. Which indicate that the yield strength of Graphene deposited Silicon is significantly improved (see **Table 1**) as compared to Silicon alone.

Bonding Graphene on the Silicon surface provides additional constraints for the surface atoms of Silicon. Deformed configuration in **Figure 4d** shows a perfect arrangement of Silicon atoms even after the application of 0.255 strain. The distribution of stress in **Figure 4d** indicate that Graphene atoms possess higher stresses, compared to the Silicon atoms. A closeup of the bond failure on the top right corner is provided in **Figure 4d**, where the first

bond failure in Graphene system is noticed. The broken atomic bonds are indicated by the dashed lines. A close look at the closeup indicates that three carbon atoms participate in bonding with underlying Silicon atoms. Continued loading results in the crack growth in Graphene and the Silicon atoms, leading to the readjustment of atoms to attain a minimum potential energy configuration, see **Figure 4e**. Further loading leads to a rapid failure in Graphene and as well as in Silicon, as shown **Figure 4f**. From **Figure 5a** and **Figure 5c**, as the crack length increases, the magnitude of potential energy of Graphene deposited Silicon remains constant for crack lengths greater than $0.15L$. Also, the strain at the first drop in the potential energy is also constant. On the other hand, as shown in **Figure 5b** and **Figure 5d**, the stress at the first bond breakage is observed to decrease with increase in crack length ($a > 0.15L$) more or less at the constant strain. Therefore, depositing Graphene on the Silicon surface is efficient in arresting crack growth in Silicon.

The variation of stress and potential energy with strain for the Graphene deposited Silicon with an initial notch (case 3) are plotted in **Figure 6a-b**, respectively. In this case, size of initial notch in Graphene is equal to the size of initial notch in Silicon. Because of the presence of initial notch in Graphene, the potential energy and stress exhibits a continuous decrease with increase in the initial crack length. The atomic configurations corresponding to a 20% initial crack size, $a = 0.2L$ are plotted in **Figure 4g-i**, which denotes the deformed configurations captured at specific points of time equal to 25.53 ps, 26.45 ps and 31.3 ps and strains values of 0.163, 0.168 and 0.199, respectively. The first bond breakage is found to occur at a strain value of 0.163, which is slightly less than the strain at the time of first bond breakage in case of the Silicone alone (0.165). Whereas, the stresses at the time of first bond breakage are much larger compared to the un-notched Silicon, refer to **Figure 3b** and **Figure 6b**. The deformed configuration at the time of first bond breakage shows crack growth in both Silicon and Graphene simultaneously, see **Figure 4g**. With continued loading, the crack continues to grow as shown in **Figure 4g-i**. The potential energy and stress at the time of first

bond breakage is inversely related to the initial crack size for case 1 and case 3. However, this is not true for case 2.

In order to further understand the mechanics of bond breakage, the atomic interactions in the three different cases are closely analysed. As mentioned in “Modelling and simulation” section, the total system potential energy E^{total} is a summation of three type of atomic interactions: (i) Silicon-to-Silicon (Si-Si) $E^{\text{Si-Si}}$, (ii) Carbon-to-Carbon (C-C) $E^{\text{C-C}}$ and (iii) Silicon-to-Carbon (Si-C) $E^{\text{Si-C}}$, which is given by:

$$E^{\text{total}} = E^{\text{Si-Si}} + E^{\text{C-C}} + E^{\text{Si-C}}, \quad (1)$$

where the last term in **Equation 1** represent the interaction energy due to the bonding between the Silicon and Carbon atoms, known as the bonding energy. Similarly, the total stress can be divided into three components, given by:

$$\sigma^{\text{total}} = \sigma^{\text{Si-Si}} + \sigma^{\text{C-C}} + \sigma^{\text{Si-C}}, \quad (2)$$

where the last term in **Equation 2** indicate the stresses induced due to the bonding between Silicon and Carbon. The individual energy terms $E^{\text{Si-Si}}$ and $E^{\text{C-C}}$ are estimated based on the atomic interaction energy of Silicon and Carbon atoms, respectively. The energy component $E^{\text{Si-C}}$ is estimated by reconsidering the atomic configuration in two different types. First, considering the Carbon atoms as the neighbours of Silicon atoms and secondly, ignoring the Carbon atoms as the neighbour of Silicon atoms. Therefore, the difference between the total energy in these two cases gives the binding energy $E^{\text{Si-C}}$. The stresses $\sigma^{\text{Si-C}}$ are also estimated following the similar lines.

Based on the distribution of the three components of potential energy and stress in **Equation 1-2** vs. strain for case 2 and case 3, the yield properties at the time of first bond breakage are estimated. The extracted yield properties are plotted for case 2 and case 3 in **Figure 7**. **Figure 7a** indicate the variation of the fracture strain with the initial crack size. When un-notched Graphene is deposited on an initially notched Silicon (case 2), the fracture strain is observed to be almost constant for initial crack lengths greater than $0.15L$. A close up

of **Figure 7a** (inset of **Figure 7a**), where a slow decrease in the fracture strain with increase in crack length is noticed. From **Figure 7a**, a fracture strain of Silicon-to-Silicon atoms is slightly on the higher side compared to the fracture strains of Carbon-to-Carbon and Silicon-to-Carbon atoms. Therefore, breakage of first bonds in the composite system happens at the least fracture strain among the possible interactions.

Bond breakage is generally initiated at the time of first drop in the potential energy/stress. The reason for the drop in case of the Graphene deposited Silicon could be breakage of first bond in Silicon-to-Silicon or Carbon-to-Carbon or Silicon-to-Carbon. The first bond failure can be estimated by examining variation of the individual terms of potential energy/stress with strain. The variation of stress and potential energy at first bond breakage are plotted in **Figure 7b-c**. For example: consider the case of Graphene deposited Silicon (case 2) with an initial crack length in Silicon equal to $0.05L$, the first drop in Silicon slab is found at a strain of 0.399 and the first drop in Graphene sheet is observed at a strain of 0.456. The stress at failure for this case in Silicon and Graphene are found to be 20.528 GPa and 60.954 GPa, respectively. On the other hand, the first drop in Silicon-to-Carbon interactions is observed at the strain of 0.456 and the corresponding stress value of -8.260 GPa. Furthermore, the total stress shows the first drop at the strain of 0.399, which is also strain value of the first drop in stress for the Silicon slab alone. Therefore, the first failure is appeared in Silicon-to-Silicon in case of the un-notched Graphene deposited Silicon system with an initial notch size equal to $0.05L$. For a system with an initial crack size of $0.1L$ in Silicon of case 2, the first drop in total stress is found to happen at a strain value of 0.303. The first drop in the stress for Carbon-to-Carbon interactions is also found to at the same strain value of 0.303. Therefore, we confirm that the first drop in the total stress is based on the least value corresponding to the first drop of stress among all the interactions. Moreover, the fracture properties for case 2 system are found to be stable for crack lengths greater than $0.15L$ crack in Silicon. The reason for this is that the Graphene used in case 2 is notch free, which creates a unique Silicon-to-

Carbon bonding interaction environment with increasing crack lengths in Silicon. Such similar bonding is subjected to tensile load leads to a first failure in the Graphene sheet for initial crack lengths in Silicon greater than $0.15L$. This is confirmed with the bonding energy at fracture in **Figure 7d** for Silicon-to-Carbon interactions.

The bonding energy in case 2 shows a constant value at -0.092 eV/atom for initial notch greater than $0.15L$ in Silicon (see **Figure 7d**). In case 3, the bonding energy is decreasing with the increase in notch size. As shown in **Figure 4d**, Carbon atom participates in bonding with three neighbor Silicon atoms. In order to consider the initial crack in the simulation, the atomic interactions are ignored between the lower and upper regions of crack. Consider a Carbon atom near to the crack surface in case 3, it has a bonding silicon neighbors on either side of the crack surface. Because of the ignored interactions, the bonding energy calculation considers only the interactions if Carbon and Silicon are one side of the crack surface. As the crack length increases, Carbon atoms lose their silicon neighbors which reduce the bonding energy. However, in case 2, graphene does not have initial notch and there exist an interaction with its neighbor silicon atoms. This creates a stable bonding environment which is confirmed with the constant bonding energy in **Figure 7d**. Such stable bonding environment maintains the fracture properties ([constant fracture strain](#) as shown in **Figure 7d**) in case 2 even with larger crack lengths in Silicon.

A comparison of the potential energy and stress along the y direction for the three different cases considered in this study are plotted in **Figure 8a-b**, respectively. Sample without crack and initial notch sizes of $0.05L$ and $0.3L$ are considered for comparison. According to **Figure 8**, an undamaged Graphene deposited on the Silicon surface always posses the highest fracture strength. Therefore, depositing Graphene on Silicon will definitely enhance the mechanical strength of Silicon used in the photovoltaic solar cells. Furthermore, considering the excellent electrical properties of Graphene, strengthening Silicon by

depositing Graphene can also replace the fingers and bus-bars used to trap the generated electrical power on Silicon based solar cells.

The influence of Graphene orientation on the Silicon surface is studied by orienting the Graphene along 0° , 15° and 30° , an initial notch size equal to $a = 0.30L$. The distribution of the potential energy and the stress along the y direction for the considered three different orientations are plotted in **Figure 9a-b**, respectively. According to **Figure 9**, the fracture strength of the composite is maximum when the Graphene is oriented along 30° .

Silicon is an anisotropic crystal, where the Young's modulus strongly depends on the crystal orientation with respect to the loading direction. For example, the Young's modulus of Silicon in [001], [110] and [111] orientations are: 130.2, 168.9 and 187.5 GPa, respectively.^[53,54] Therefore, the influence of anisotropy of Graphene deposited Silicon is also studied here, considering an initial crack length of $0.2L$. The variation of stress and potential energy for case 1 for different Silicon orientations are shown in **Figure 10**. The stress-strain curves in **Figure 10a** highlights the influence of anisotropy of Silicon, where the slope of the curves is observed to be increasing with respect to the crystal orientation in the order of [001], [011], [111]. According to **Figure 10a** the fracture strength is observed to be highest for [111] orientation, for all the cases. On the other hand, the effect of anisotropy is not significant in the potential energy per atom curves, see **Figure 10b**.

Furthermore, Silicon at different orientations is coated with Graphene and the fracture analysis is extended the composite system. The results of cases 2 and 3 are also superimposed in **Figure 10a-b**. Based on **Figure 10a** the fracture strength of Graphene deposited Silicon in case 2 is observed to be higher than the cases 1 and 3. Moreover, the fracture strength of when Silicon is observed along [111] direction is found to be the highest for case 2. On the other hand, the corresponding increase in fracture strength when Silicon is oriented along [111] direction in case 2 is 362%, when compared to the same orientation in of Silicon in case 1. The surface Silicon atoms in case 1 are not having their full set of neighbors to achieve a

stable equilibrium. This makes the system into energetically unstable. In case 2, deposited Graphene atoms participate bonding with Silicon and this interaction improves the system stability (changes in the potential energy for case 1 and case 2 in **Figure 10b**). This stable system possess significant enhancement in the fracture properties compared to case 1. The increase in fracture strength for [111] orientation of Silicon is 17%, as compared to the [001] orientation, for case 2. The number of free atoms on the Silicon surface is a function of crystal orientation. From [001] to [111] orientations of Silicon, the number of atoms are increased from 1683 to 2347. The increase in number of Silicon atoms involve in increasing the bonding density with Graphene. The increased bonding density further enhanced the fracture properties.

4. Conclusions

The influence of depositing Graphene on Silicon surface on the enhancement in fracture properties has been studied based on molecular dynamics simulations. Various types of interactions between the Silicon and Carbon atoms in Graphene are modeled using the combination of AIREBO and Tersoff potential functions. To pin-point the influence of depositing Graphene on Silicon, MD simulations are performed considering three different cases: (i) notched Silicon alone, (ii) notched Silicon deposited with defect free Graphene and (iii) notched Silicon deposited with Graphene containing initial notch. The fracture strength is estimated based on the first failure, which is identified using the individual interaction contributions from Silicon and Carbon.

The fracture properties of Graphene deposited Silicon demonstrated significant improvement in the fracture properties, as compared to the Silicon alone. The Young's modulus is found to be increased about 780% for case 2, i.e., notched Silicon deposited with defect free Graphene. Furthermore, simulations indicated that the un-notched Graphene can arrest the crack growth in Silicon, even with large initial crack sizes. Unique bonding

environment is identified in un-notched Graphene coated Silicon, which helps in maintaining consistent fracture properties. The influence of Graphene orientation on the Silicon surface is also studied and we report that the fracture strength of the composite is maximum when the Graphene is oriented along 30° . Furthermore, the fracture strength of the monolithic and composite systems, when Silicon is oriented along [111] direction is found to be the highest in all cases. The increase in fracture strength is found to be 17%, when Silicon is oriented along [111] direction in case 2, as compared to that of case 1. Therefore, we report the definite improvement in mechanical and fracture properties of Silicon when coated with Graphene.

Acknowledgements

BJ and XZ are gratefully acknowledging the sponsorship from Sofja Kovalevskaja Programme of Alexander von Humboldt Foundation.

Received: ((will be filled in by the editorial staff))

Revised: ((will be filled in by the editorial staff))

Published online: ((will be filled in by the editorial staff))

References

- [1] F. Meillaud, M. Boccard, G. Bugnon, M. Despeisse, S. Hänni, F.-J. . Haug, J. Persoz, J.-W. Schüttauf, M. Stuckelberger, C. Ballif, *Mater. Today* **2015**, 18, 378.
- [2] M. Paggi, S. Kajari-Schröder, U. Eitner, *J. Strain Anal. Eng. Des.* **2011**, 46, 772.
- [3] M. Green, K. Emery, Y. Hishikawa, W. Warta, E. Dunlop, *Prog. Photovoltaics Res. Appl.* **2014**, 22, 701.
- [4] D. You, S. H. Kim, H. Lee, J.-W. Chung, S.-T. Hwang, Y. H. Heo, S. Lee, H.-M. Lee, *Prog. Photovoltaics Res. Appl.* **2015**, 23, 973.
- [5] NREL, *{NREL} Solar Cell Sets World Efficiency Record at 40.8 Percent*; 2008.
- [6] A. Goetzberger, C. Hebling, H.-W. Schock, *Mater. Sci. Eng. R* **2003**, 40, 1.
- [7] M. Ye, X. Wen, M. Wang, J. Icozzia, N. Zhang, C. Lin, Z. Lin, *Mater. Today* **2015**, 18, 155.
- [8] Y. Aya, W. Shinohara, M. Matsumoto, K. Murata, T. Kunii, M. Nakagawa, A. Terakawa, M. Tanaka, *Prog. Photovoltaics Res. Appl.* **2012**, 20, 166.
- [9] H. Simon, B. Grégory, P. Gaetano, B. Mathieu, E. Jordi, D. Matthieu, M. Fanny, B. Christophe, *Prog. Photovoltaics Res. Appl.* **2013**, 21, 821.
- [10] M. Foti, C. Tringali, A. Battaglia, N. Sparta, S. Lombardo, C. Gerardi, *Sol. Energy Mater. Sol. Cells* **2014**, 130, 490.
- [11] J. Alok, S. Richa, P. Hardik, P. Nilesh, R. Sharma, *J. Phys. D. Appl. Phys.* **2015**, 48, 275101.
- [12] D. Das, A. Banerjee, *Appl. Surf. Sci.* **2015**, 345, 204.
- [13] H. Babar, E. Abasifreke, I. Ferguson, *Sol. Energy Mater. Sol. Cells* **2015**, 139, 95.

- [14] N. Park, J. Jeong, C. Han, *Microelectron. Reliab.* **2014**, *54*, 1562.
- [15] M. Köntges, I. Kunze, S. Kajari-Schröder, X. Breitenmoser, B. Bjrnklett, *Sol. Energy Mater. Sol. Cells* **2011**, *95*, 1131.
- [16] T. Pletzer, J. Mülken, S. Reißland, O. Breitenstein, K. Joachim, *Prog. Photovoltaics Res. Appl.* **2015**, *23*, 428.
- [17] M. Paggi, I. Berardone, A. Infuso, M. Corrado, *Sci. Rep.* **2014**, *4*, 4506.
- [18] S. Rein, K. Bothe, B. Sattler, *FVS, BSW-Solar* **2007**, 120.
- [19] A. Barron, *Mater. Today* **2015**, *18*, 2.
- [20] S. Kajari-Schröder, I. Kunze, M. Köntges, *Energy Procedia* **2012**, *27*, 658.
- [21] S. Schröder, I. Kunze, M. Köntges, *Energy Procedia* **2012**, *27*, 658.
- [22] J. Käsewieder, F. Haase, M. Larrodé, M. Köntges, *Energy Procedia* **2014**, *27*, 469.
- [23] I. Berardone, M. Corrado, M. Paggi, *Energy Procedia* **2014**, *55*, 22.
- [24] H. Yang, H. Wang, D. Cao, D. Sun, X. Ju, *Int. J. Photoenergy* **2015**, *2015*, 251615.
- [25] P. Budarapu, B. B Javvaji, V. Sutrar, D. Mahapatra, G. Zi, T. Rabczuk, *J. Appl. Phys.* **2015**, *118*, 382.
- [26] D. H. Lee, J. Yi, J. M. Lee, S. J. Lee, Y. J. Doh, H. Y. Jeong, Z. Lee, U. Paik, J. A. Rogers, W. Il Park, *ACS Nano* **2013**, *7*, 301.
- [27] S. Sahu, G. C. Rout, *Int. Nano Lett.* **2017**, *7*, 81.
- [28] A. Suhail, G. Pan, D. Jenkins, K. Islam, *Carbon*. **2018**, *129*, 520.
- [29] X. Li, H. Zhu, K. Wang, A. Cao, J. Wei, C. Li, Y. Jia, Z. Li, X. Li, D. Wu, *Adv. Mater.* **2010**, *22*, 2743.
- [30] X. An, F. Liu, Y. J. Jung, S. Kar, *Nano Lett.* **2013**, *13*, 909.
- [31] S. Riazimehr, A. Bablich, D. Schneider, S. Kataria, V. Passi, C. Yim, G. S. Duesberg, M. C. Lemme, *Solid. State. Electron.* **2016**, *115*, 207.
- [32] Q. Huang, M. J. Loveridge, R. Genieser, M. J. Lain, R. Bhagat, *Sci. Rep.* **2018**, *8*, 1.
- [33] S. Kobayashi, Y. Anno, K. Takei, T. Arie, S. Akita, *Sci. Rep.* **2018**, *8*, 1.
- [34] D. H. Shin, S. Kim, J. M. Kim, C. W. Jang, J. H. Kim, K. W. Lee, J. Kim, S. D. Oh, D. H. Lee, S. S. Kang, C. O. Kim, S. H. Choi, K. J. Kim, *Adv. Mater.* **2015**, *27*, 2614.
- [35] M. Paggi, A. Saporita, *Energy Procedia* **2013**, *38*, 506.
- [36] J. Gow, C. Manning, *IEEE Proceedins Electr. Power Appl.* **1999**, *146*, 193.
- [37] M. Paggi, M. Corrado, M. Rodriguez, *Compos. Struct.* **2013**, *95*, 630.
- [38] S. Plimpton, *J. Comput. Phys.* **1995**, *117*, 1.
- [39] S. J. Stuart, A. B. Tutein, J. A. Harrison, *J. Chem. Phys.* **2000**, *112*, 24903.
- [40] J. Tersoff, *Phys. Rev. B* **1989**, *39*, 5566.
- [41] C. D. Latham, A. J. McKenna, T. P. Trevethan, M. I. Heggie, M. J. Rayson, P. R. Briddon, *J. Phys. Condens. Matter* **2015**, *27*, 316301.
- [42] B. Javvaji, S. Raha, D. R. Mahapatra, *J. Nanoparticle Res.* **2017**, *19*, 31.
- [43] A. K. Rappé, C. J. Casewit, K. S. Colwell, W. A. Goddard Iii, *J. Am. Chem. Soc.* **1992**, *114*, 10024.
- [44] Z. Wang, K. Bi, H. Guan, J. Wang, *J. Mater.* **2014**, *2014*, 1.
- [45] X.-M. Qin, T.-H. Gao, W.-J. Yan, X.-T. Guo, Q. Xie, *J. Mol. Struct.* **2014**, *1061*, 19.
- [46] B. Javvaji, B. M. Shenoy, D. R. Mahapatra, A. Ravikumar, G. M. Hegde, M. R. Rizwan, *Appl. Surf. Sci.* **2017**, *414*, 25.
- [47] J. Hermann, R. A. DiStasio, A. Tkatchenko, *Chem. Rev.* **2017**, *117*, 4714.
- [48] T.-T. Nguyen, A. Ambrosetti, S. Bordas, A. Tkatchenko, *Bull. Am. Phys. Soc.* **2018**.
- [49] Y. Y. Zhang, Q. X. Pei, C. M. Wang, *Appl. Phys. Lett.* **2012**, *101*, 081909.
- [50] Y. Y. Zhang, C. M. Wang, Y. Cheng, Y. Xiang, *Carbon N. Y.* **2011**, *49*, 4511.
- [51] R. Grantab, V. B. Shenoy, R. S. Ruoff, **2010**, *946*, 2.
- [52] H. Zhao, K. Min, N. R. Aluru, *Nano Lett.* **2009**, *9*, 3012.
- [53] J. Kim, D. (Dan) Cho, R. S. Muller, In *Transducers '01 Eurosensors XV*; (Ed. E.

Obermeier) Springer Berlin Heidelberg: Berlin, Heidelberg, Germany 2001, pp. 662–665.

[54] M. a Hopcroft, W. D. Nix, T. W. Kenny, *J. Microelectromechanical Syst.* 2010, 19, 229.

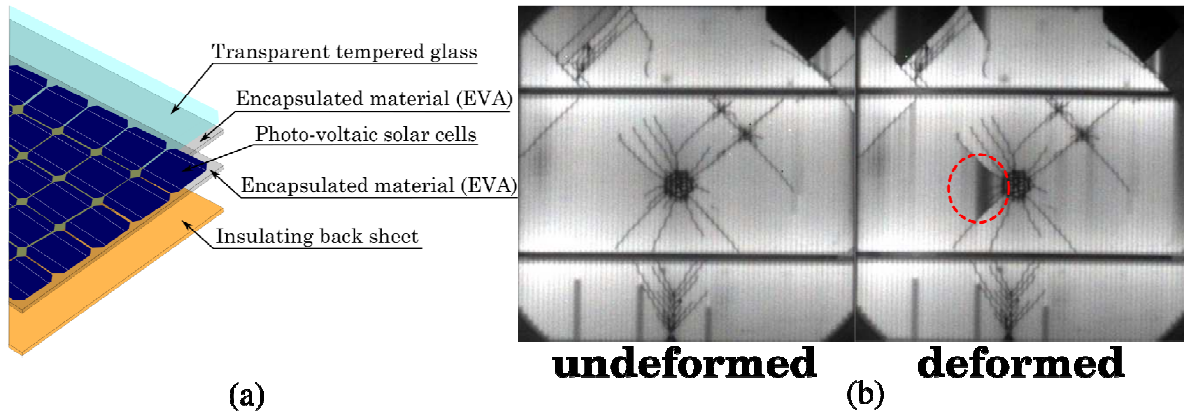


Figure 1. (a) Different layers of a photovoltaic module. (b) Electric response and crack pattern of a solar cell: flat/undeformed and loaded/deformed configuration, reproduced with permission.^[17]

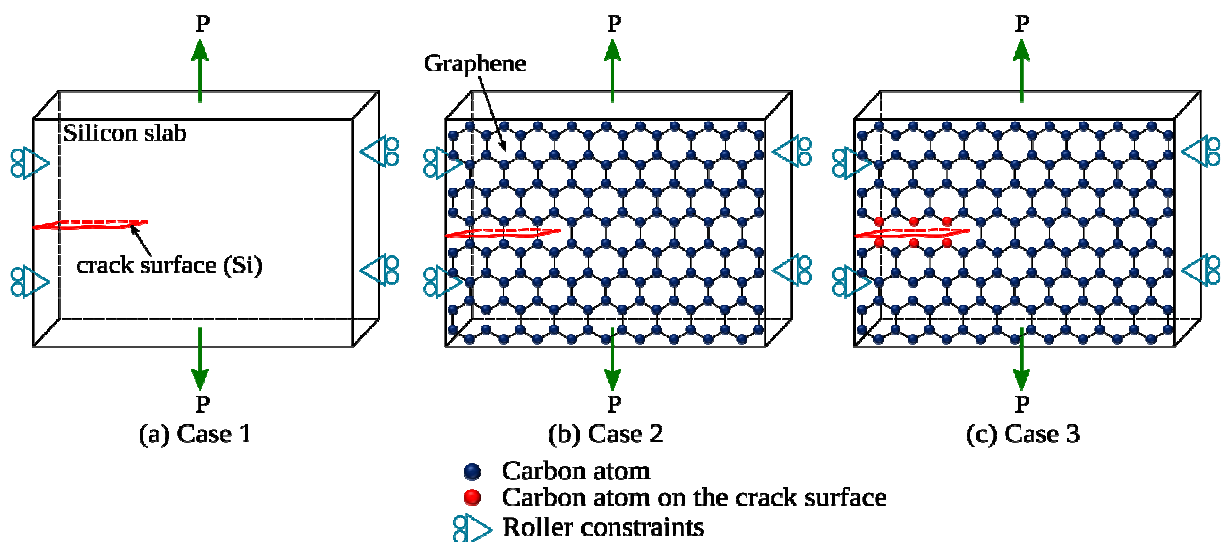


Figure 2. Three different cases simulated in the present study. (a) Case 1: fracture simulations of Silicon alone. (b) Case 2: Silicon with a un-notched Graphene on the surface and (c) Case 3: initial edge notched Silicon, deposited with an initial edge notched Graphene

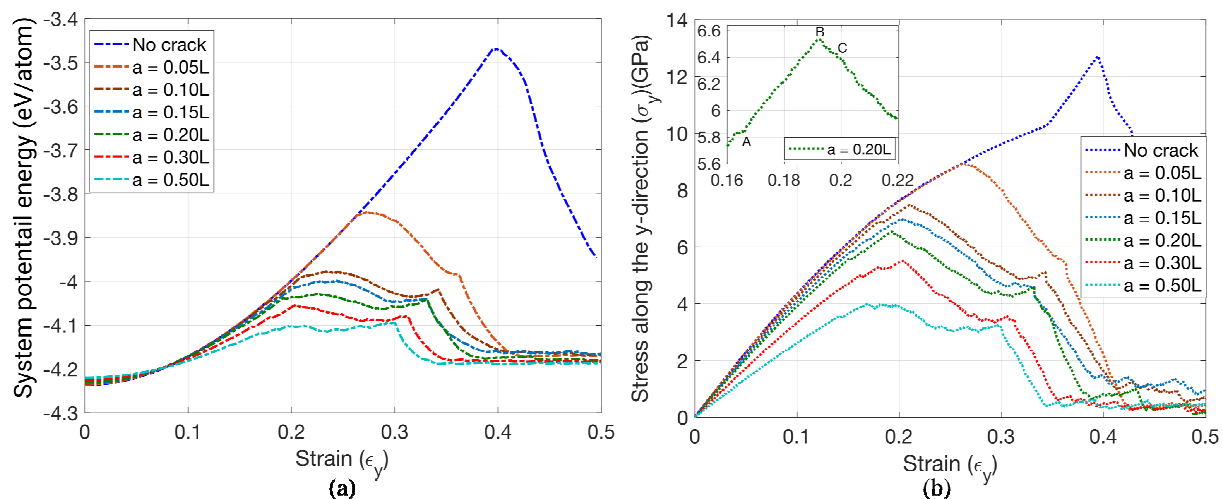


Figure 3. Distribution of the (a) system potential energy and the (b) stress along y-direction (σ_y) for various initial notch sizes vs. the strain along the y-direction (ϵ_y) for Silicon alone (case 1), see Figure 2a.

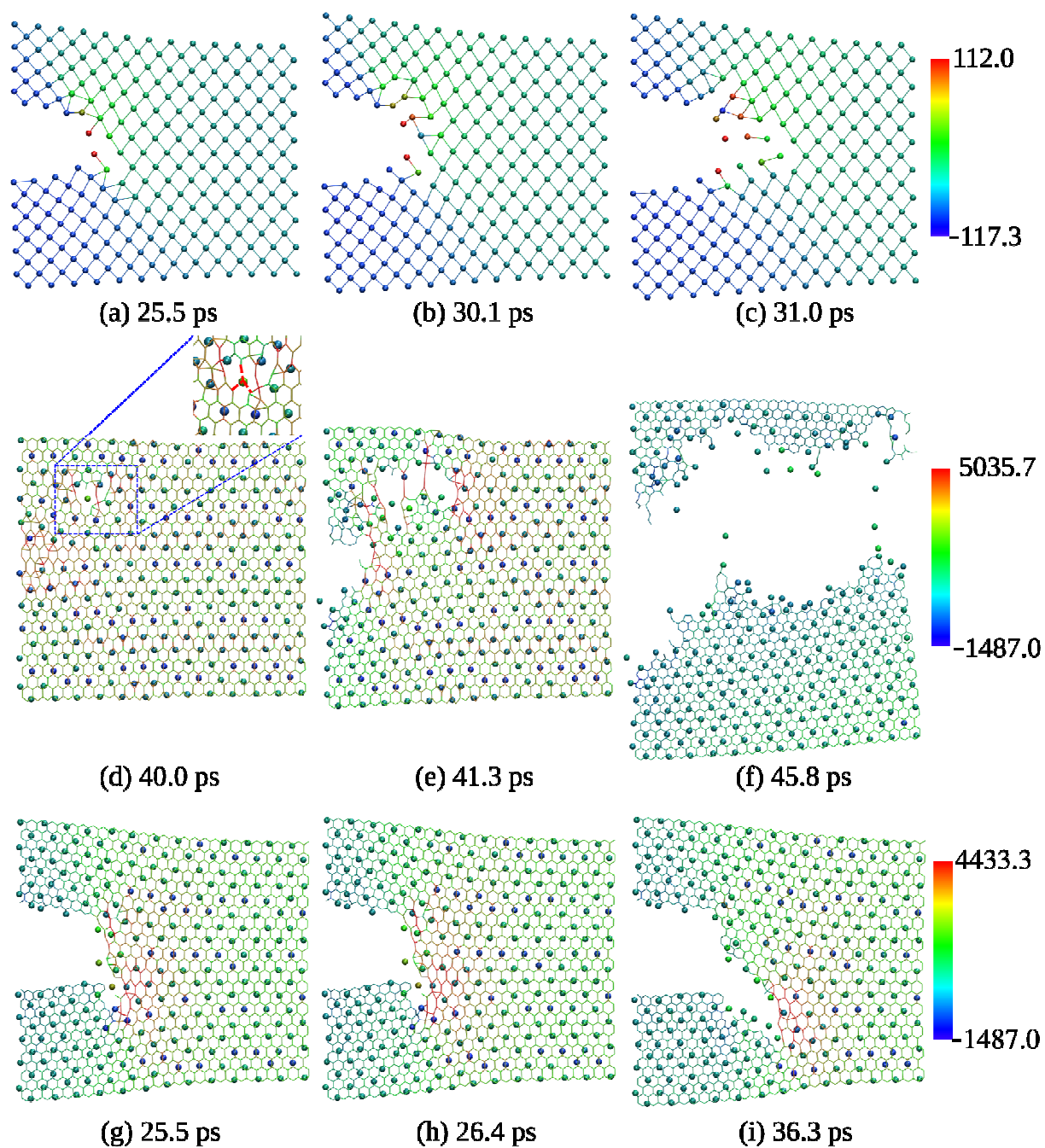


Figure 4. Deformed configurations of the three different cases (see **Figure 2**) at various time, considering an initial notch size $a = 0.20L$. Bond breaking and crack growth in (a-c) case 1, (d-f) case 2 and (g-i) case 3. The closeup of (d) represents the first bond failure in Graphene.

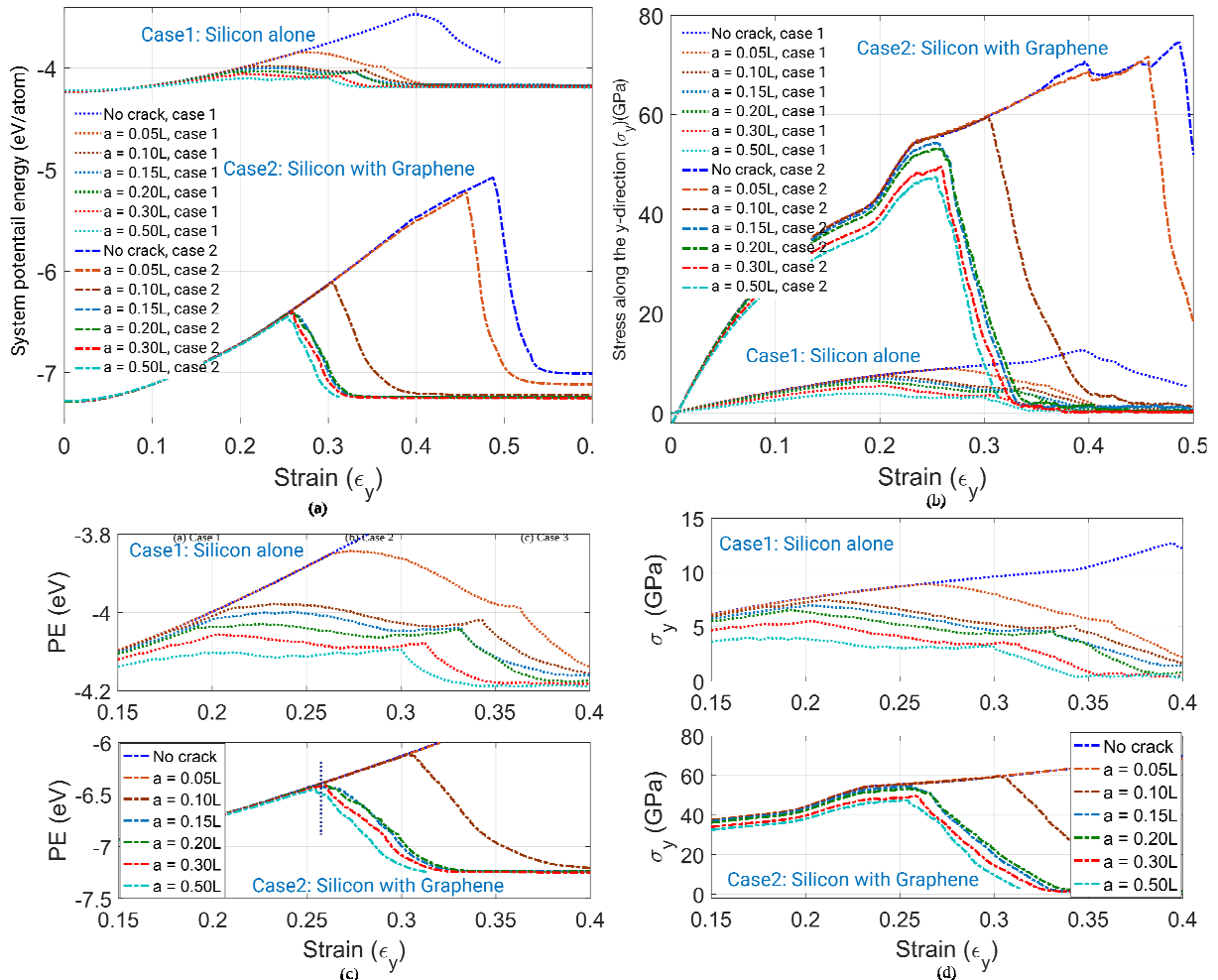


Figure 5. Comparison of the (a) potential energy and (b) the stress along the y-direction for Graphene deposited Silicon (case 2) and Silicon alone (case 1) cases. Close ups in the strain range 0.15-0.4, of (a) and (b) are shown in (c) and (d), respectively.

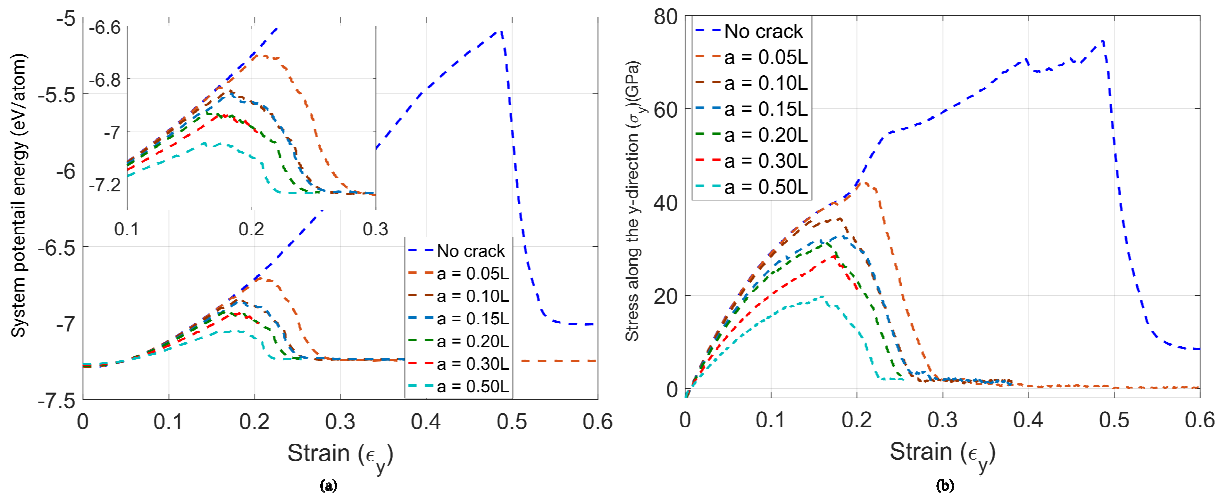


Figure 6. Distribution of the (a) system potential energy and the (b) stress along the y-direction (σ_y) for various initial notch sizes vs. the strain along the y-direction (ϵ_y) for case 3, see Figure 2c.

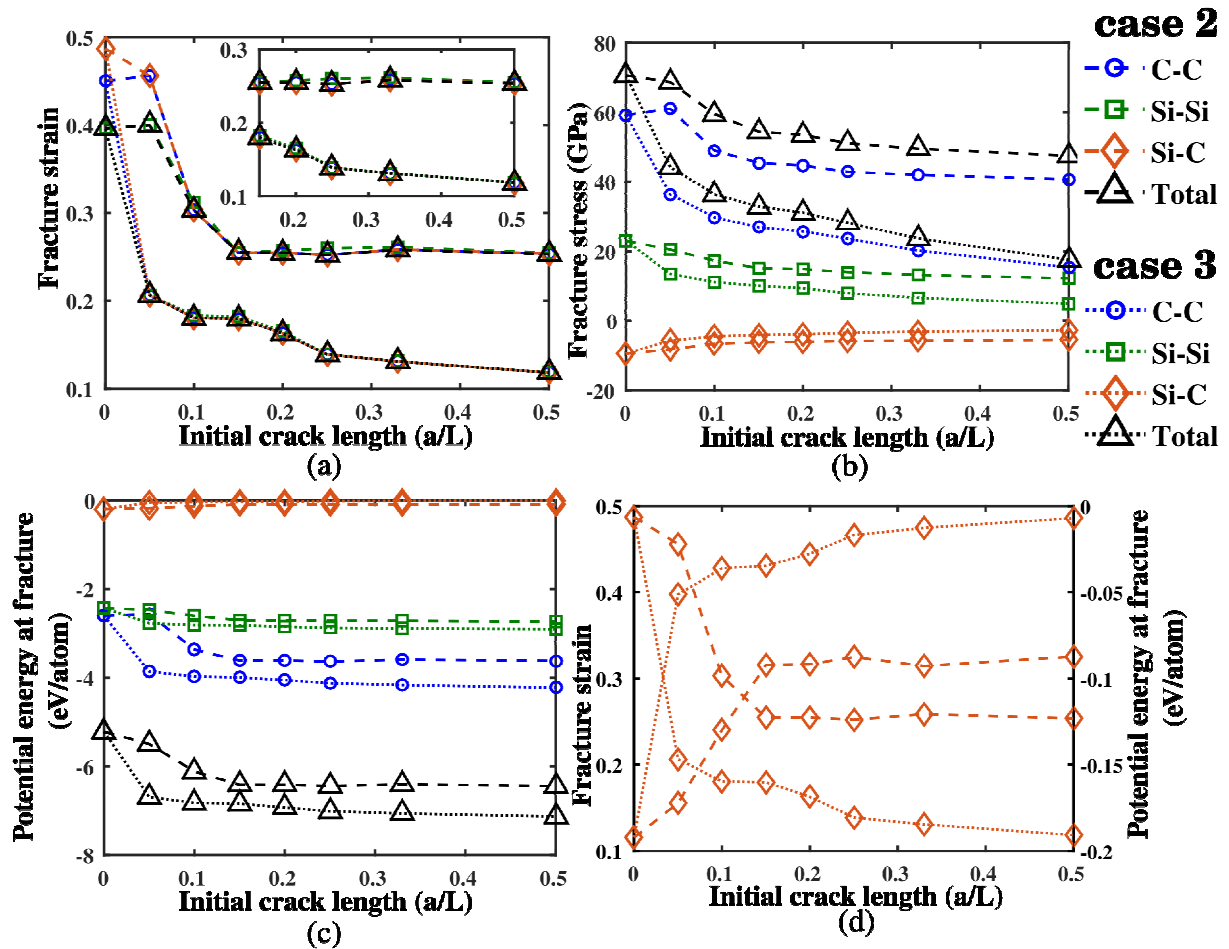


Figure 7. Fracture properties for case 2 and case 3. Variation of (a) fracture strain (b) fracture stress and (c) potential energy at fracture with initial crack length. (d) The contribution of Silicon-to-Carbon interaction to the fracture strain and potential energy at fracture with initial crack length. Dashed lines indicate the results of case 2 and dotted lines represent the results of case 3 systems. Marker circles, squares, diamonds and triangles correspond to Carbon-to-Carbon, Silicon-to-Silicon, Silicon-to-Carbon and total interactions, respectively.

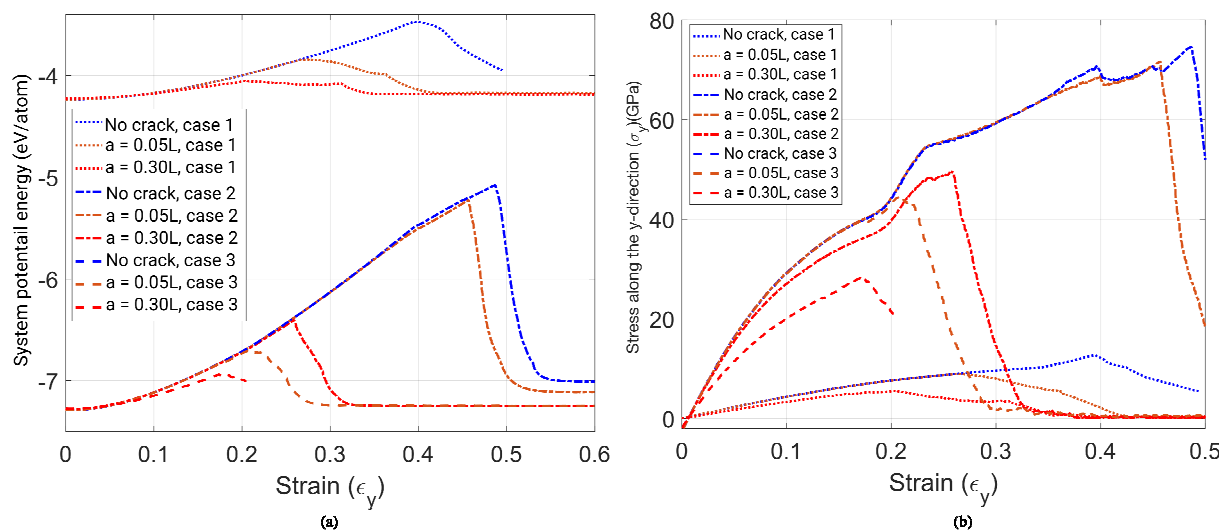


Figure 8. The potential energy and the stress along the y-direction for cases 1-3 are compared in (a) and (b), respectively.

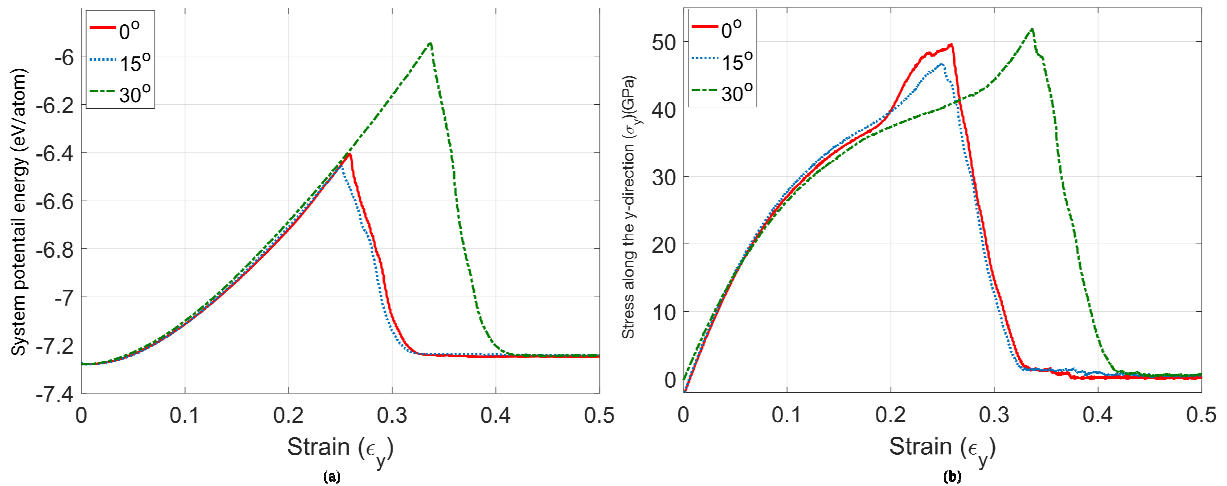


Figure 9. Distribution of the (a) system potential energy and the (b) stress along the y-direction when Graphene is oriented along 0° , 15° and 30° for case 2, (see **Figure 2b**) with an initial notch size equal to $a = 0.30 L$.

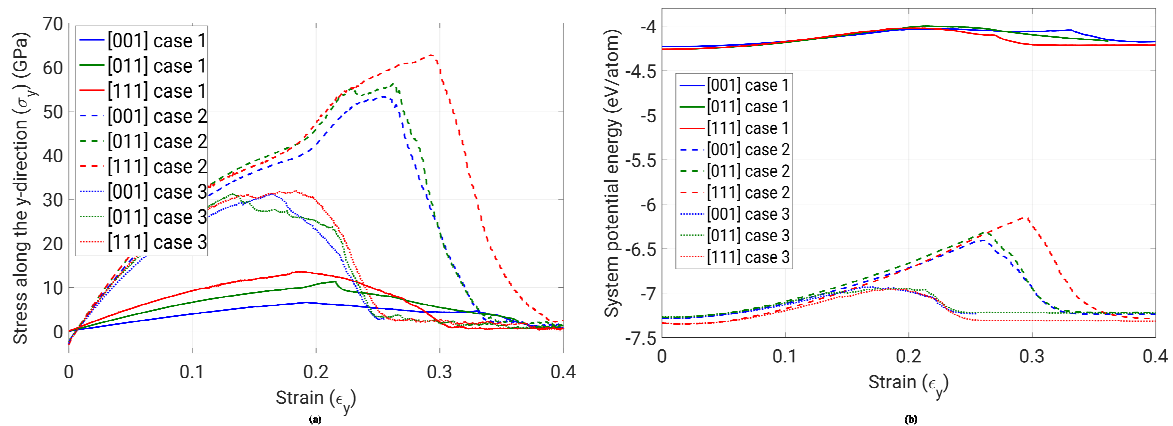


Figure 10. Distribution of the (a) stress along the y-direction and the (b) system potential energy for cases 1 to 3 with an initial notch size $0.2L$ for different Silicon orientations. Solid, dashed and dotted lines indicate the responses for case 1, case 2 and case 3, respectively.

Table 1. Young's modulus distribution for various cases

Case	Young's modulus (GPa)
Si alone, no crack ($a = 0$)	44.90
Si alone, 20% initial crack ($a = 0.2L$)	41.26
Graphene deposited Si, no crack ($a = 0$)	384.20
Graphene deposited Si, 20% initial crack in Si ($a = 0.2L$)	365.85
Graphene deposited Si, 20% initial crack in both Si and Graphene ($a = 0.2L$)	327.78

The table of contents entry should be 50–60 words long, and the first phrase should be bold.

Molecular dynamics simulations explored the enhancement in fracture properties for Graphene coated Silicon compared to Silicon alone. Detailed analysis of the bonding and non-bonding interactions between Carbon and Silicon explore the possibility of first bond failure in the combined system. The Graphene coating controls the crack propagation in Silicon based photovoltaic cells.

Keyword

B. Javvaji, P. R. Budarapu*, M. Paggi*, X. Zhuang, T. Rabczuk

Fracture properties of Graphene-coated Silicon for photovoltaics

ToC figure ((Please choose one size: 55 mm broad × 50 mm high or 110 mm broad × 20 mm high. Please do not use any other dimensions))

